JOURNAL OF AIRCRAFT
Vol. 39, No. 4, July–August 2002

Control of a Miniducted-Fan Unmanned Aerial Vehicle Using Active Flow Control

Pearl Haiyan Fung*
Georgia Institute of Technology, Atlanta, Georgia 30332
and
Michael Amitay†
Georgia Tech Research Institute, Smyrna, Georgia 30080

An experimental study of the control of the flowfield around the stator vanes of a new miniducted-fan unmanned aerial vehicle (UAV) using synthetic jet actuators is presented. As a result, a new control approach of the UAV is proposed in which active flow control can be used instead of moving control surfaces and articulated rotor blade. Therefore, the UAV's propulsion and control systems are reduced to a single moving part, a fixed pitch propeller. This mechanical simplicity makes the active flow control application particularly attractive for development of mini- and micro-UAVs. The directional and rotational control of the UAV (0.5 m in diameter and 0.15 m in height) can be obtained by controlling the flow within the duct. This can be achieved by the activation of surface fluidic actuators based on synthetic jet technology that are located downstream from a miniature passive obstruction. The synthetic jets are flush mounted on a set of four fixed stators located downstream from the propeller. In the present work the flowfield around the stator vanes is studied using particle image velocimetry at different radial locations, where the geometrical angle of attack of the stator vanes is fixed at 10 deg and the propeller rotational speed is either 4300 or 6200 rpm. Velocity measurements in the near wake are also obtained, and the data show that as a result of the actuation the cross-stream extent of the wake and its velocity deficit are significantly reduced and the flow is quasi-steady.

Introduction

UNMANNED aerial vehicles (UAVs) possess much potential for the ever-growing technological world. UAVs offer low cost flights, portability, and simplicity of operation. It is therefore an important task to fully understand and develop the control of the UAV. The directional control of a UAV can be accomplished by controlling the flow around the UAV. The present work concentrates on the control of a vertical takeoff and landing (VTOL) mini-UAV with a ducted-fan configuration. A new approach to control the UAV by actively controlling the flow within the duct, via synthetic jet fluidic actuators, is proposed.

A ducted-fan vehicle is based on the principles of a helicopter; they are both VTOL vehicles. A ducted-fan configuration is superior in a UAV design because its duct or shroud provides a safety measure to the ground operator and observers. Furthermore, the duct prevents the propeller from coming into contact with any object, and the enclosing of the propeller also improves its static thrust efficiency.

The directional and rotational control of a ducted-fan UAV is typically obtained by using mechanical devices such as control vanes or counter-rotating rotors. In 1986, Sikorsky Aircraft Corporation started their development on its Cypher UAV.[1,2] The Cypher uses two coaxial counter-rotating four-blade rotors for control and stabilization. (The rotors are controlled by a ground operator.) The Cypher uses collective and cyclic pitch on the rotor blades to control lift and moments about the three-body axes. The rotors provide torque equilibrium and a means of directional control. The pitching motion of the aircraft is accomplished by twisting rectangular flexbeams, where the directional motion is accomplished by using differential collective.

Another ducted fan UAV (iSTAR[3,4]) was developed by Micro Craft Incorporated. The propulsion of the iSTAR is generated by a two-blade propeller powered by a commercial-off-the-shelf engine. Eight fixed stators are placed downstream of the propeller to reduce the engine torque. Directional control of the craft is provided by the control vanes attached to the trailing edge of the stators. The control vanes are actuated by four servos placed inside the duct. Brynestad[5] and Moran[6] also utilized control vanes for their vehicle control. The vehicle Brynestad and Moran used had the body of a conventional aircraft but extracts its thrust from a single ducted fan installed in the center of the craft. The ducted fan could be tiled horizontally or vertically for forward or vertical flights, respectively. The ducted fan had four fixed stator vanes to which control vanes are attached at the trailing edge. Because of the use of fixed wings (for directional control), the main purpose of the stator vanes is to straighten the wake beneath the duct.

Kondor and Heiges[7] used circulation control using steady jet injection via a pneumatic blowing ring mounted on the base of the duct. The blowing ring has a nonmoving round trailing-edge slot through which a sheet of airjet is supplied by a compressed air system. The sheet of air stayed attached to the curved trailing edge by a balance between the negative pressure differential across the jet and the centrifugal force acting on the curving jet. In addition, four fixed stator vanes were installed to partially counter the torque caused by the main rotor and provide structural support of the body. The directional and rotational control techniques just described are either mechanically complex[1–4] or require external compressed air.[7]

In the present work active flow control with synthetic jet actuators is proposed to control the direction and rotation of the vehicle. The operation of synthetic jet actuators is described in detail in an earlier paper of Smith and Glezer.[8] Nominally a plane turbulent airjet is synthesized by a train of two-dimensional vortex pairs. The vortices are formed at the edge of an orifice by the motion of a small diaphragm mounted at the bottom of a sealed shallow cavity. In the

Received 18 June 2001; revision received 26 November 2001; accepted for publication 26 March 2002.

*Graduate Student, School of Mechanical Engineering; fun_guy315@hotmail.com.

†Research Engineer, Aerospace, Transportation and Advanced Systems Laboratory; michael.amitay@me.gatech.edu.

present experiments circular diaphragms are driven at resonance in a shearing mode by a centrally mounted piezoceramic disks. During the forward motion of the diaphragm, fluid is ejected from the cavity, and the ensuing flow separates at the sharp edge of the orifice forming a vortex sheet. This vortex sheet then rolls into a vortex pair that begins to move away from the orifice under its own self-induced velocity. When the diaphragm begins to move away from the cavity, the vortex is sufficiently removed and is thus unaffected by the ambient fluid that is drawn into the cavity. Although during each cycle the net mass flux out of the cavity is zero, each vortex pair has a finite hydrodynamic impulse (or momentum) into the flow. Therefore, when a synthetic jet is mounted within a surface the interaction between the jet and the crossflow can lead to the formation of a closed recirculating flow region, which displaces the local streamlines and thus modifies the pressure distribution on the surface.

The use of synthetic (zero-mass-flux) jet actuators for controlling the flow around airfoils was demonstrated by Smith et al.[9] and Amitay et al.,[10,11] where the suppression of separation over an unconventional airfoil at moderate Reynolds numbers (up to 10^6) was obtained, which resulted in a dramatic increase in lift and a corresponding decrease in pressure drag. The synthetic jets were deliberately operated at frequencies that were typically an order of magnitude higher than the characteristic (shedding) frequency of the airfoil. These authors argued that the interaction of high-frequency zero-net-mass-flux jets with the crossflow leads to local modification of the "apparent" aerodynamic shape of the flow surface and, as a result, to full or partial reattachment of the separated flow.

Chatlynne et al.[12] and Amitay et al.[13] utilized synthetic jet actuators for the concept of virtual aeroshaping. The work was performed on a thick (24%) two-dimensional Clark-Y airfoil model at low angles of attack where the baseline flow is completely attached to the surface of the airfoil. Their idea was to activate a synthetic jet actuator that was placed downstream of a passive obstruction to form a recirculating domain. The formation of this domain altered the streamline resulting in the modification of the apparent shape of the airfoil and improving the aerodynamic performance of the airfoil at low angles of attack.

In the present paper a new UAV control technique is suggested in which the directional and rotational control of the vehicle can be obtained by controlling the flow within the duct by actively controlling the flow around the stator vanes. This results in alteration of the aerodynamic forces on the vanes, which in return alters the forces and moment around the entire vehicle. The technique involves the activation of spanwise synthetic jet actuators mounted in fixed stator vanes of a ducted mini-UAV. This technique is based on the work of Chatlynne et al.[12] and Amitay et al.,[13] where the flow over the stator vanes is forced to separate using a mini-passive obstruction and is reattached using a spanwise synthetic jet actuator. Thus, by controlling the flow around each stator vane separately (and different from each other) the directional and rotational control can be achieved.

Experimental Setup and Procedure

The UAV is sized for 10 min of hovering or slow speed translating flight at maximum gross weight, with a 20% gross weight payload allowance, which places the vehicle in the 2–3 kg class. Two full-scale models were constructed to investigate the design issues. A full-scale, three-dimensional stationary model was designed and constructed to investigate the effects of synthetic jet actuation on the flow within a ducted fan and especially on the flow around the stator vanes. The second (dynamic) model, having 5 degrees of freedom, was built as a proof of concept of the UAV design and the control scheme. In the present paper the results of the first model are presented.

The model consists of a propeller and four stator vanes that are contained within a duct (Fig. 1). Each stator is instrumented with a spanwise (plane) synthetic jet actuator to alter the flow around it. The model is attached to a frame such that it is 1.5 m above the ground to minimize ground effects. The duct is made out of an aluminum sheet metal with an inner diameter of 0.3 m. Two styrofoam pieces resembling the shapes of the inlet and outlet of

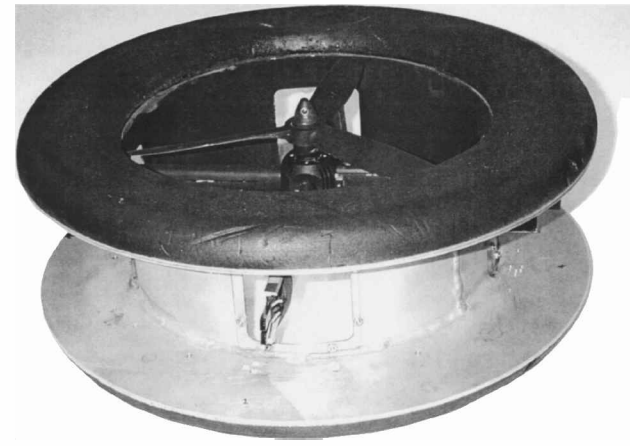

Fig. 1 Stationary miniducted-fan UAV.

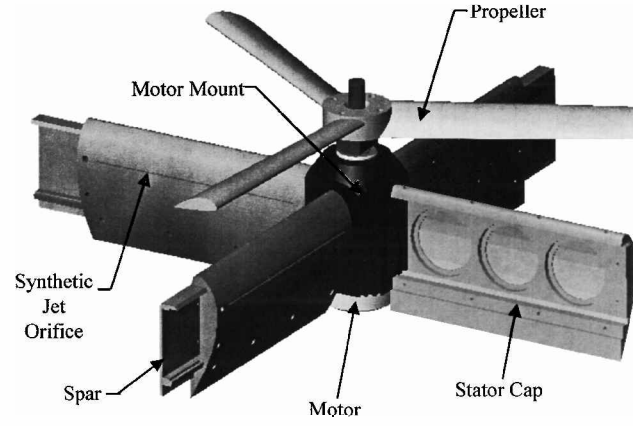

Fig. 2 UAV drive system assembly.

the UAV are attached to the duct. On the circumference of the duct are four square openings for flow visualization and particle image velocimetry (PIV) data collection of the flowfield around the stators.

The flow within the duct is produced by a commercial off-the-shelf three-blade propeller for model airplanes. The propeller is driven by a brushless dc motor and solid-state switching controller, fed with a dc power supply. The motor controller is regulated by a pulse-train waveform, where the rotational speed is varied by changing the width of the pulse. For protection purposes in the event of a loose propeller during operation, four Plexiglas® shields of thickness 4.4 mm were placed on the four sides of the frame.

Four stator vanes are located 25.4 mm downstream of the propeller and at 90 deg from each other (Fig. 2). Each stator vane has a 24% thickness ratio Clark-Y cross section with a chord of $c = 63.5$ mm and is comprised of two parts, a cap and a spar. The caps are made from stereo lithography, whereas the spars are machined by electric discharge machining. Each stator vane is instrumented with an individually addressable synthetic jet actuator having an orifice of width 0.5 mm and length 109 mm along the radial direction. The slits are located at different streamwise locations on the stator vanes, at distances $x_j = 8.6$, 15.9, 24.4, and 31.9 mm from the leading edge, with corresponding nondimensional streamwise locations $x_j/c = 0.135$, 0.25, 0.38, and 0.50. (In the experiments reported here the effect of the first two slit locations was tested.) Each synthetic jet actuator is driven by three piezoceramic disks that are preselected to have the same resonance frequency (allowing a variation of ± 10 Hz). Each stator vane cap is designed to provide a common cavity for the three disks, whereas the spar is used to hold the disks. The stator vanes are attached to the motor mount and also provide structural support for the UAV.

The flow data within the duct are acquired using the PIV technique. The PIV system consists a pair of 50 mJ Nd:Yag lasers, two lenses (a −50 FL cylindrical lens and a 1000-mm spherical lens), a Newport mirror that is placed on a traverse on the bottom of the

frame to direct the laser onto the stator vane, a charge-coupleddevice camera for capturing the images, and a LaserPulse synchronizer to synchronize between the lasers and the camera.

The flowfields over the stator vanes and in the near wake are measured at eight normalized radial locations $r/R = 0.09$, 0.17, 0.26, 0.35, 0.44, 0.52, 0.61, and 0.700. (r is the radial distance from the center of the duct, and R is the inner radius of the duct.) The data are comprised of 300 image pairs and are taken with time delays between the two lasers of 20 or 5 μs (for the global or detailed views, respectively). The uncertainty of the velocity measured using PIV is $\pm 3\%$, whereas the uncertainly in the vorticity is $\pm 5\%$.

The synthetic jet actuator performance is quantified using the momentum coefficient c_μ, which is the ratio of the synthetic jet momentum flux to the freestream momentum flux,

$$c_\mu = \frac{\rho_j b U_j^2}{\frac{1}{2}\rho_0 c U_\infty^2}$$

where ρ_j and ρ_0 are the jet and freestream fluid densities, respectively; b is the jet orifice width; c is the chord of the stator vane; U_j is the jet peak velocity measured at 1 mm downstream of the jet orifice; and U_∞ is the freestream velocity. Here, the freestream velocity is measured at $y = 0.4c$ above the stator. However, because the freestream velocity is radially nonuniform the average freestream velocity (of the eight radial locations) is used to calculate the momentum coefficient. In the experiments reported here the synthetic jet is actuated at 1040 Hz, and $c_{\mu_{av}} = 1.84 \times 10^{-3}$ and 8.8×10^{-4} for $\omega = 4300$ and 6200 rpm, respectively. Note that the frequency associated with the time of flight is $\sim$20 Hz, which is more than an order of magnitude smaller than the actuation frequency, resulting in a quasi-steady reattachments. (For details on the effects of the actuation frequency, see Amitay et al.[11] and Amitay and Glezer.[14])

Results

Baseline Configuration

The effect of the actuation on the flowfield above the surface of the stator vane is investigated using PIV in the x–y plane at eight radial locations along the stator vane ($r/R = 0.09$–0.70 at intervals of $\Delta r/R = 0.09$). In the results reported next the data for only three radial locations are presented ($r/R = 0.26$, 0.44, and 0.70, marked in Fig. 3 as a, b, and c, respectively). Each image measures 60 mm on the side and consists of 300 realization pairs, in which the field of view is restricted to the suction side of the airfoil. Here, the geometric angle of attack of the stator is fixed at 10 deg, the propeller rotation speed is either 4300 or 6200 rpm, and the synthetic jet actuator is located at $x_j/c = 0.14$ or 0.25, with a nominal jet velocity of 15 m/s ($C_{\mu av} = 1.84 \times 10^{-3}$ and 8.80×10^{-4} for $\omega = 4300$ and 6200 rpm, respectively).

Figures 4a–4f show the time-averaged velocity vector maps at three radial locations for the baseline flow (Figs. 4a–4c) and with actuation at $x_j/c = 0.25$ (Figs. 4d–4f), where the propeller rotation speed is 4300 rpm. In the absence of control, the flow at $r/R = 0.26$ and 0.44 (Figs. 4a and 4b, respectively) is completely attached to the suction side of the stator vane. However, at $r/R = 0.7$ (Fig. 4c) the flow is separated near the trailing edge at $x/c > 0.80$. When actuation is applied at $x_j/c = 0.25$ (Figs. 4d–4f, marked by the arrows), the velocity vector fields above the surface of the airfoil at $r/R = 0.26$ and 0.44 appear to be qualitatively similar to the corresponding velocity fields in the absence of the control (Figs. 4a and 4b). At $r/R = 0.70$ (Fig. 4f) actuation results in a slight increase in the separated region (that is, the separation point moves from $x/c = 0.80$ to 0.68). Note that actuation at $x_j/c = 0.14$ (not shown) resulted in similar effects.

The effect of propeller rotation speed is also investigated for $\omega = 6200$ rpm and jet actuation at $x_j/c = 0.25$ (Figs. 5a–5f). The flowfields at the higher rotational speed appear to be qualitatively similar to those at the corresponding locations at the lower rpm (Figs. 4a–4f) except that the velocity magnitude is higher by $\sim$40% with respect to the lower rpm caused by the higher downwash velocity from the propeller. The jet velocity remains the same for all of the cases; thus, the momentum coefficient is reduced by $\sim$50% for the higher rotational speed case suggesting that actuation at a smaller jet momentum coefficient has similar effects to the higher momentum coefficient. This result is consistent with the measurements of Chatlynne et al.[12] on a two-dimensional airfoil.

Combined Obstruction-Synthetic Jet

As is shown in the preceding section, for $\omega = 4300$ and 6200 rpm the baseline flow fields at the various radial locations are either completely or partially attached to the surface of the stator vane. Consequently, the effect of the synthetic jet actuation (at either $x_j/c = 0.14$ or 0.25) is very small. To achieve a substantial effect of the actuation on the flow over the stator vanes (and consequently to modify the aerodynamic performance of the ducted-fan UAV), a different method is used. It is based on the work of Chatlynne et al.[12] and Amitay et al.[13] on a two-dimensional Clark-Y airfoil model. The approach is to induce separation on the stator vane at a desired streamwise location by placing a small passive obstruction on the suction side of the stator vane. Actuation of synthetic jet actuator that is placed downstream from the obstruction forms a stationary

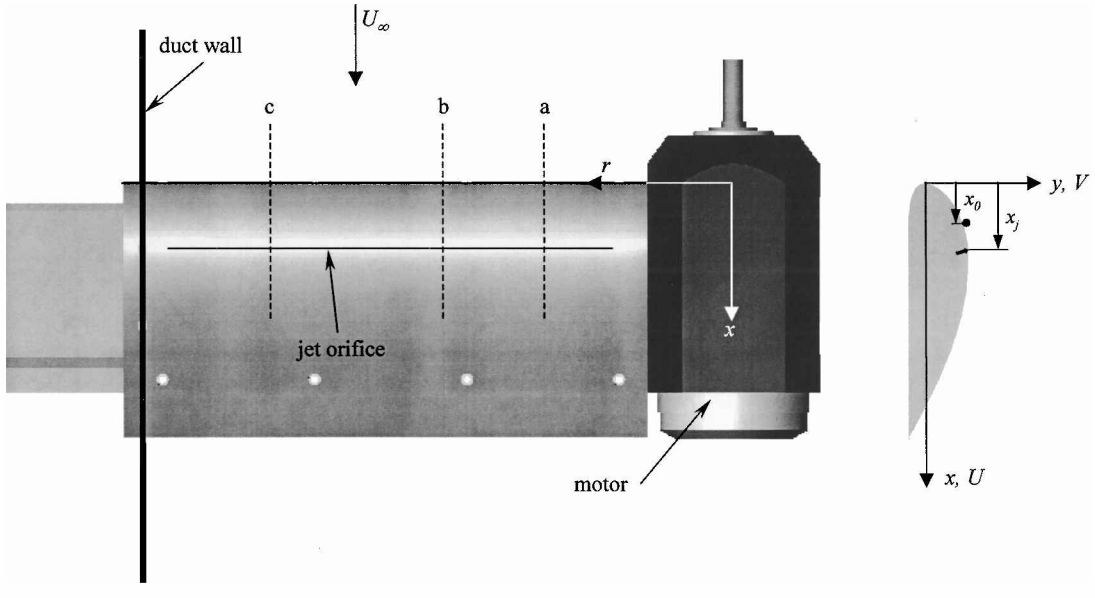

Fig. 3 Radial measurement locations and coordinate system definition.

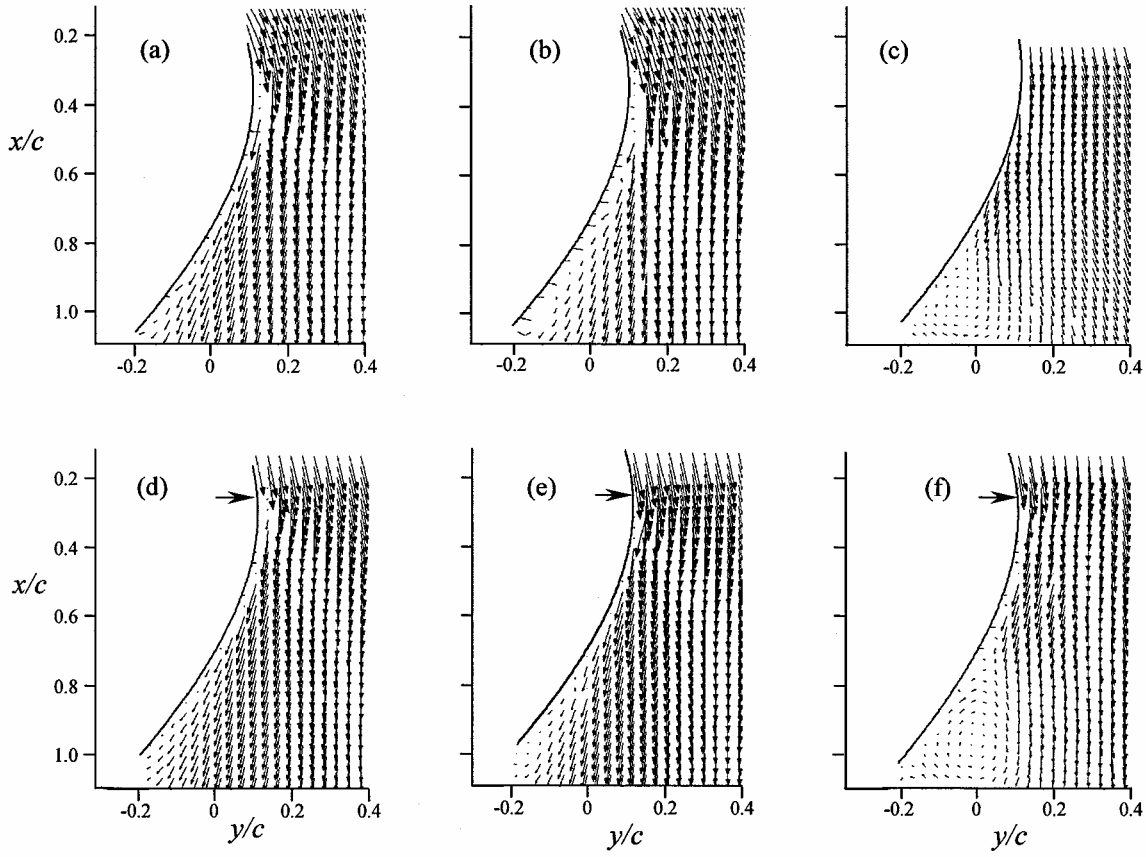

Fig. 4 Cross-stream maps of the velocity vectors at $\omega = 4300$ rpm. Baseline: a) $r/R = 0.26$, b) 0.44, and c) 0.70; actuation at $x_j/c = 0.25$: d) $r/R = 0.26$, e) 0.44, and f) 0.70.

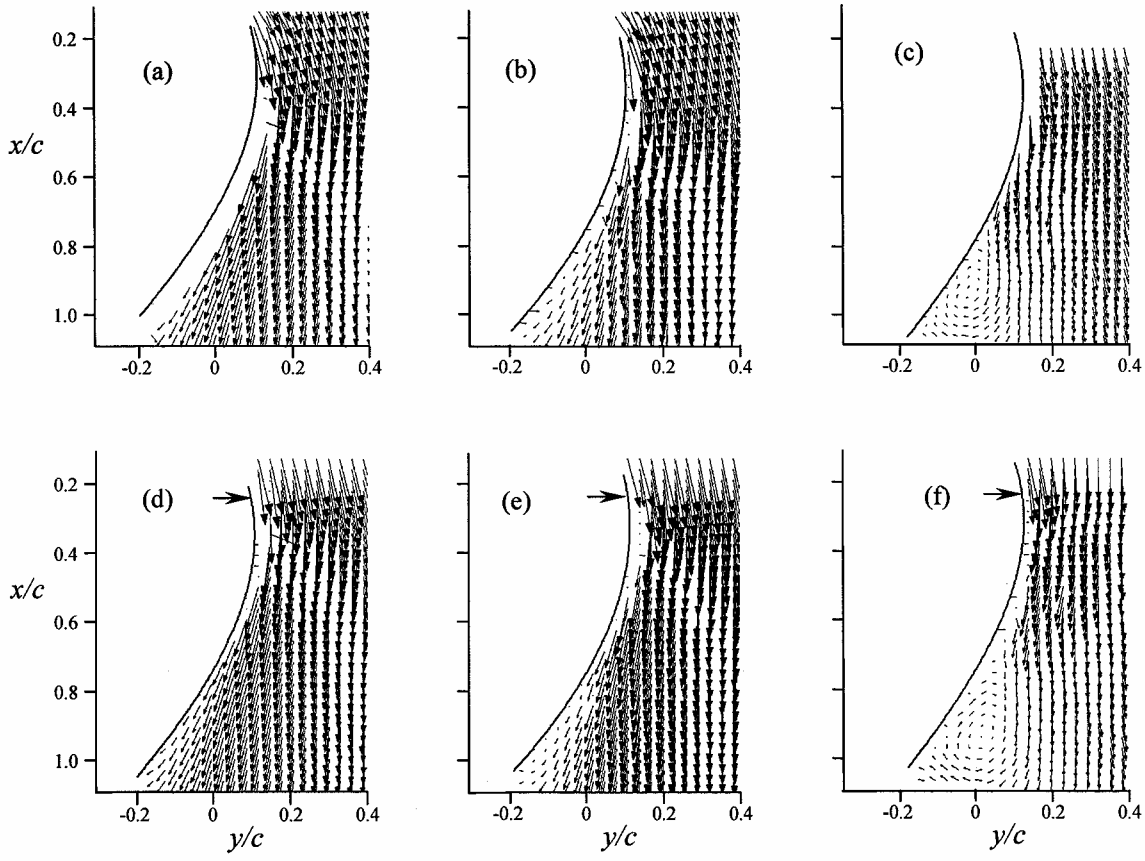

Fig. 5 Cross-stream maps of the velocity vectors at $\omega = 6200$ rpm. Baseline: a) $r/R = 0.26$, b) 0.44, and c) 0.70; actuation at $x_j/c = 0.25$: d) $r/R = 0.26$, e) 0.44, and f) 0.70.

recirculating flow domain next to the surface, which results in flow reattachment. The formation of this domain alters the flow above the airfoil by inducing a displacement of the local streamlines that is sufficient to modify the pressure distribution on the surface of the airfoil.

In what follows an obstruction of height $h/c = 0.01$ is attached to the suction side of the stator vane at either $x_0/c = 0.18$ or 0.21, and the control jets are either at $x_j/c = 0.14$ or 0.25 (upstream or downstream, respectively, of the obstruction). As was shown by Chatlynne et al.,[12] the effect of jet actuation is more prominent when the control jet is located at $x_j/c = 0.25$; hence, most of the data presented here are at this jet location. However, a limited amount of experiments was also performed for jet location $x_j/c = 0.14$ with obstruction placed at $x_0/c = 0.21$ to study the effect of the jet actuation upstream of the obstruction.

Global Views

Figures 6a–6f present the velocity vector fields of the baseline flow (Figs. 6a–6c) and actuated flow ($x_j/c = 0.25$, Figs. 6d–6f) above the stator vane at $\omega = 4300$ rpm, where the obstruction is located at $x_0/c = 0.21$. The obstruction causes flow separation above the pressure side of the stator vane at all radial locations (except at $r/R = 0.09$ and 0.17, which are closest to the center of the duct, not shown). At $r/R = 0.26$ (Fig. 6a) the flow is on the verge of separation, where the magnitude of the velocity is reduced for $x/c > 0.38$ compared to the vectors at the corresponding location when no obstruction was used (Fig. 4a), indicating a thicker boundary layer. At $r/R = 0.44$ and 0.70, Figs. 6b and 6c, respectively, the flow is separated at $x/c > 0.39$ and 0.71, respectively.

When control is applied, the flow reattaches (either completely or partially) as shown in Figs. 6d–6f. At $r/R = 0.26$, where the baseline flow is on the verge of separation (Fig. 6a), the actuated flow is completely attached (Fig. 6d). At $r/R = 0.44$ the extent of the separated region is significantly reduced when actuation is applied (Fig. 6e). At this location the separation point move from $x/c = 0.39$ to 0.71, when control is applied. However, the flowfield at $r/R = 0.70$ (Fig. 6f) remained almost unchanged with only a slight increase of the separated region from $x/c = 0.71$ (baseline flow, Fig. 6c) to $x/c = 0.72$ when control is applied.

Corresponding concentrations of the spanwise vorticity are computed from the velocity fields and are shown using gray-scale raster images in Figs. 7a–7c and 7d–7f for the baseline and actuated flows, respectively. The images of the time-averaged baseline configuration show that at $r/R = 0.26$ (Fig. 7a), where the flow is on the verge of separation, the layer of the negative (CW) vorticity concentration (that is, the cross-stream spreading of the vorticity) is very thick at $x/c > 0.6$. At the other locations (Figs. 7b and 7c), where the flow is partially separated, the CW vorticity is concentrated in the separated shear layer. Also, the vorticity field associated with the region of reversed flow on the upper surface shows a thin concentration of opposite-sense (CCW, marked by the closed line) spanwise vorticity near the surface of the airfoil. When actuation is applied, the cross-stream extent of the spanwise vorticity at $r/R = 0.26$ (Fig. 7d) is significantly reduced. At $r/R = 0.44$ (Fig. 7e) the extent of the cross-stream and streamwise extent of the CCW (representing the reversed flow) is significantly reduced. However, at $r/R = 0.7$ the vorticity field remains the same when actuation is applied.

Detailed Views

As just shown, placing the obstruction at $x_0/c = 0.21$ yields flow reattachment at most of the radial locations when the jet at $x_j/c = 0.25$ is activated. To understand the mechanisms associated with the flow reattachment, the flow in the vicinity of the combined obstruction-synthetic jet is measured in more detail.

Figures 8a–8c present the detailed ($0.17 < x/c < 0.4$) baseline velocity vector fields above the stator vane at the three radial locations ($r/R = 0.26$, 0.44, and 0.70) for $\omega = 4300$ rpm. In each plot a scaled circle represents the location and size of the obstruction. The high magnification of the vector field reveals that the flow downstream of the obstruction is locally separated. In the global view (Fig. 6a) the

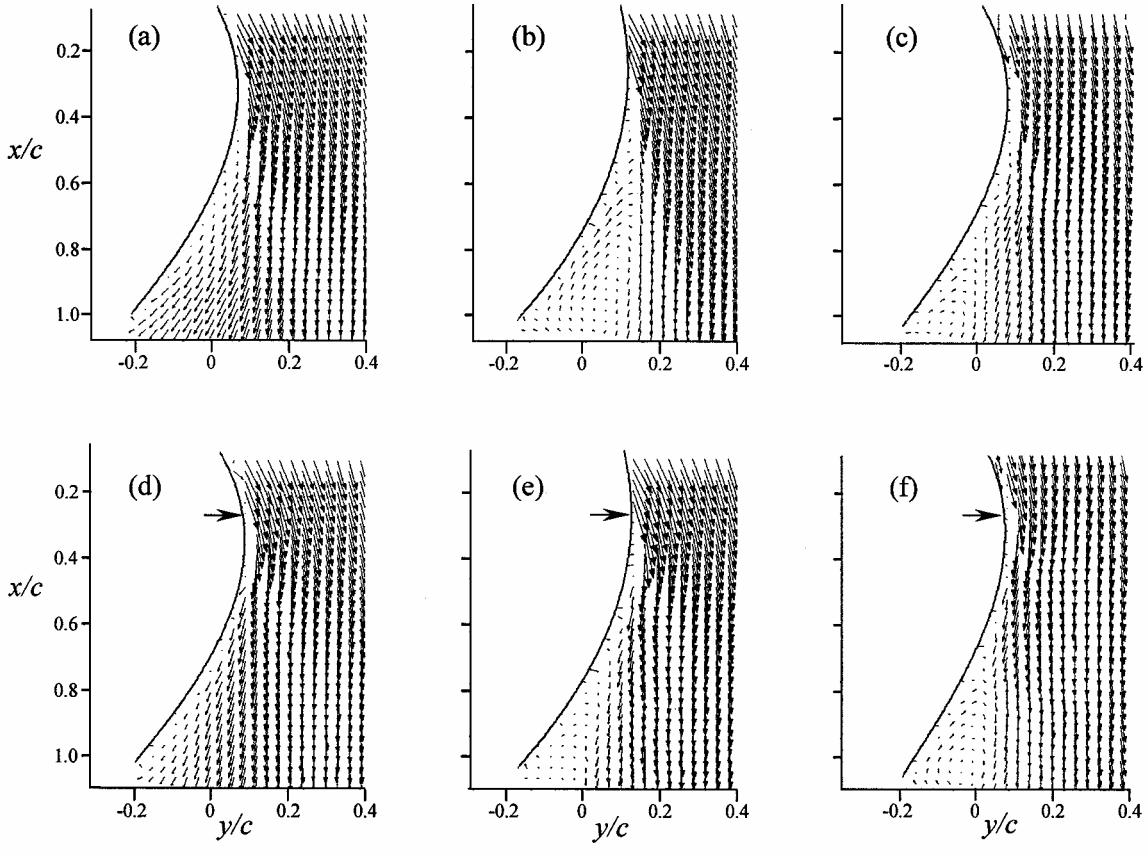

Fig. 6 Cross-stream maps of the velocity vectors with obstruction at $x_0/c = 0.21$ and $\omega = 4300$ rpm. Baseline: a) $r/R = 0.26$, b) 0.44, c) 0.70; actuated at $x_j/c = 0.25$: d) $r/R = 0.26$, e) 0.44, and f) 0.70.

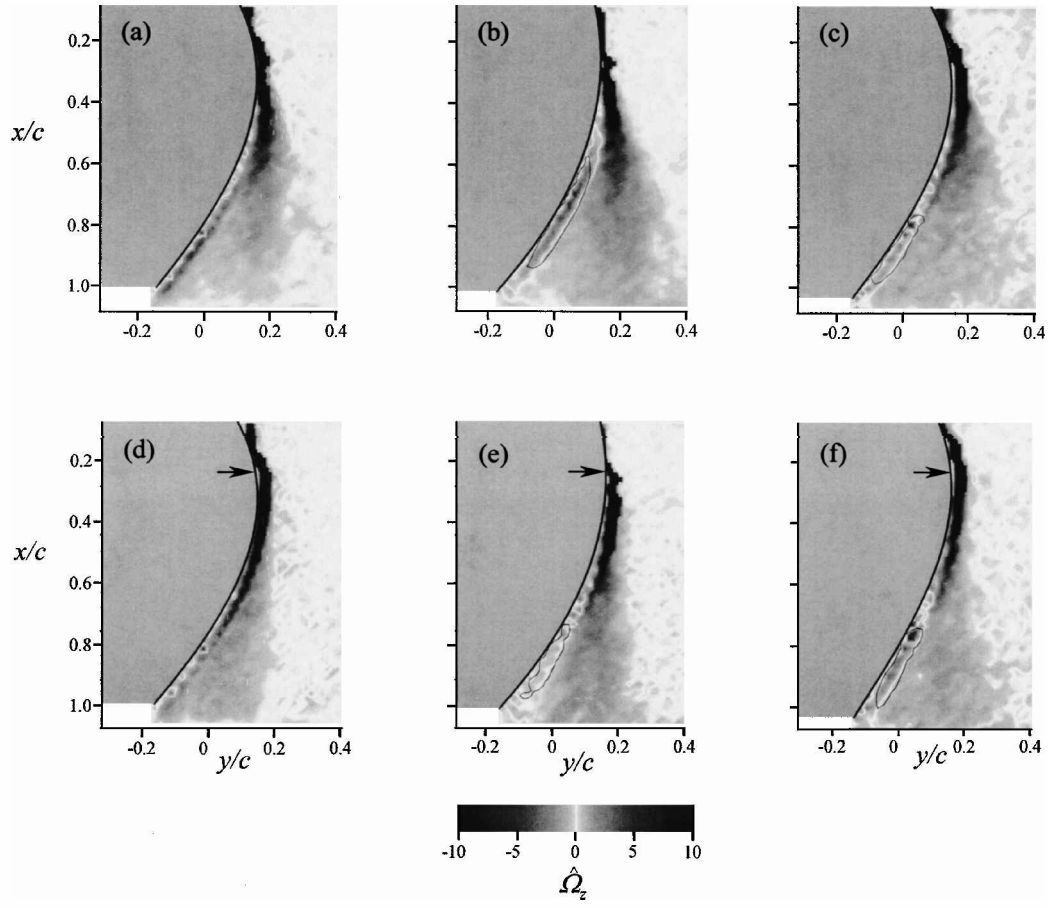

Fig. 7 Cross-stream maps of the spanwise vorticity with obstruction at $x_0/c = 0.21$ and $\omega = 4300$ rpm. Baseline: a) $r/R = 0.26$, b) 0.44, c) 0.70; actuated at $x_j/c = 0.25$: d) $r/R = 0.26$, e) 0.44, and f) 0.70.

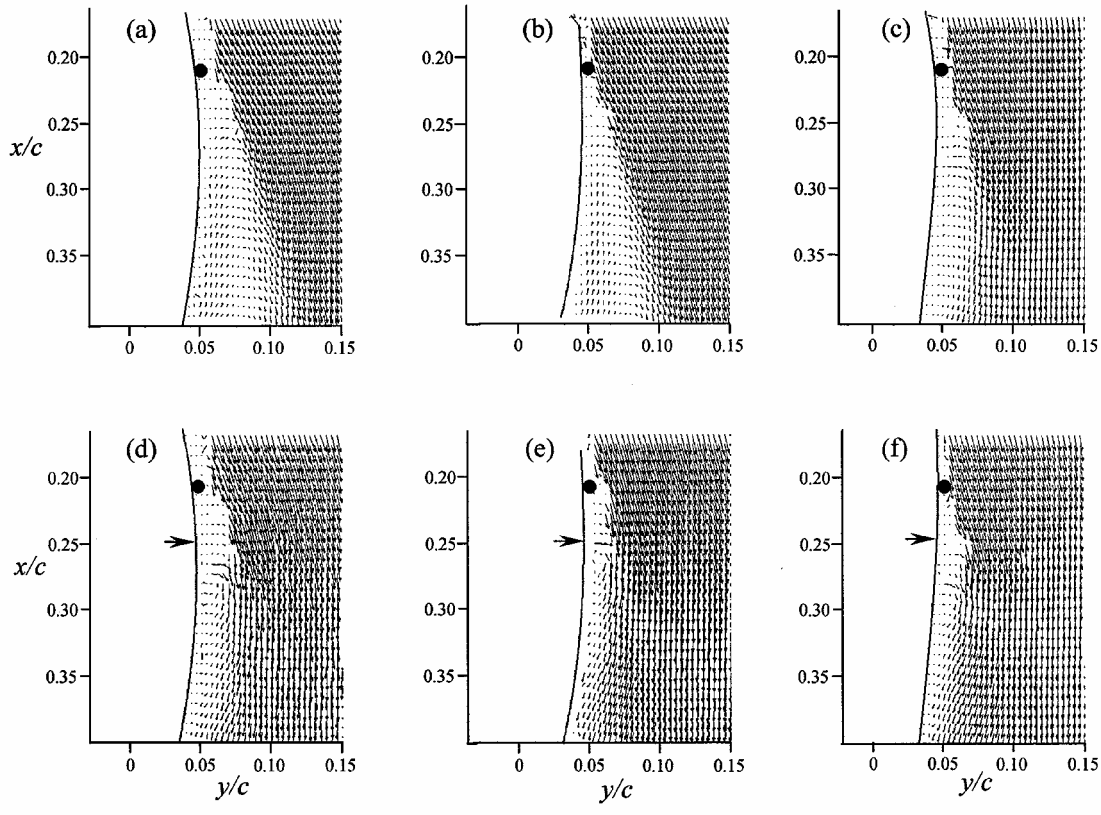

Fig. 8 Detail cross-stream maps of the velocity vectors with obstruction at $x_0/c = 0.21$ and $\omega = 4300$ rpm. Baseline: a) $r/R = 0.26$, b) 0.44, c) 0.70; actuated: d) $r/R = 0.26$, e) 0.44, and f) 0.70.

baseline flow at $r/R = 0.26$ is on the verge of separation, whereas the detailed view (Fig. 8a) reveals local separation downstream of the obstruction. The flow is also separated at the other locations (Figs. 8b and 8c). However, at $r/R = 0.70$ a closed recirculating flow domain is formed on the surface of the stator vane downstream of the obstruction. Although the field of view does not enclose the entire bubble, it is apparent that a closed domain is formed. This is evidenced by the velocity vectors that are tilted toward the surface at the domain $x/c > 0.34$ and $y/c > 0.07$.

Figures 8d–8f show the velocity vector fields in the vicinity of the combined obstruction jet when the jet at $x_j/c = 0.25$ is activated, where the arrow in each plot indicates the location of the synthetic jet. The activation of the synthetic jet results in a closed recirculating domain, where downstream of this domain the flow is completely attached to the surface of the stator. The downstream extent of the closed domain varies at the different radial locations and is equal to $x/c = 0.36$, 0.36, and 0.37 for $r/R = 0.26$, 0.44, and 0.70, respectively.

The internal structure of the recirculating bubble is also investigated using phase-averaged measurements at three phases during the actuation cycle and is shown in Figs. 9a–9c and 10a–10c (velocity vectors and spanwise vorticity, respectively). Each image is comprised of two frames each measuring 11 mm on the side. Figures 9a and 10a show the beginning of suction cycle, Figs. 9b and 10b are the beginning of the blowing cycle, and Figs. 9c and 10c are the phase at which maximum blowing occurs. At the beginning of the suction cycle (Figs. 9a and 10a), the recirculating domain includes a clockwise (CW) vortex centered approximately at $2.6 \cdot h$ downstream from the obstruction. The image also shows the separated flow downstream from the obstruction's cross-stream edge. Another CW vortex is visible farther (at $\sim 11 \cdot h$) downstream. When the blowing stroke begins (Figs. 9b and 10b), a weak CCW vortex is formed on the top-side of the jet orifice, whereas the CW vortex of the vortex pair is much larger. (The nominally two-dimensional synthetic jet forms a counter-rotating vortex pair during the blowing cycle.) At the same time the secondary (downstream) CW vortex that was formed during the preceding cycle is moving downstream, and its strength is significantly reduced. At $\phi = 252$ deg (maximum blowing, Figs. 9c and 10c) the CCW vortex is clearly visible, and the CW vortex (of the vortex pair) increases in size and is moving downstream. The second (downstream) vortex is almost completely dispersed in the freestream and is advected farther downstream. By the time the cycle repeats itself, the CW vortex (of the vortex pair) is advected outside of the downstream edge of the primary bubble, while the downstream vortex is vanished. This sequence of images clearly indicates that the streamwise extent of the bubble is of the order of two to three wavelengths of the actuation frequency (for example, based on half the local freestream velocity). More importantly, similar to the earlier observations of Honohan et al.,[15] farther downstream the actuation frequency has negligible temporal effect on the vorticity distribution within the wall boundary layer. Similar behavior (not shown) was obtained at the higher propeller rotation speed.

Effect of Jet Location

In the experiments just shown the synthetic jet is placed in the separated region (downstream of the obstruction). In the following set of data, the synthetic jet is placed upstream of the obstruction. The obstruction is at the same location as for the preceding experiments ($x_0/c = 0.21$), whereas the synthetic jet is located at $x_j/c = 0.18$. The experiments were performed at both propeller rotation speeds ($\omega = 4300$ and 6200 rpm). The cross-stream maps of the velocity field for the baseline flow at $r/R = 0.26$, 0.44, and 0.70 are replotted and shown in Figs. 11a–11c, respectively, whereas Figs. 11d–11f present the corresponding flowfields when the flow is actuated. At $r/R = 0.26$ and 0.44 (Figs. 11d and 11e, respectively) actuation results in a slight increase of the separated flow domain. At $r/R = 0.70$ (Fig. 11f) actuation results in an *increase* of the separated region, moving the separation point upstream (from $x_s/c = 0.58$ to 0.32). These results, which are in a qualitative agreement with the results for a flow over two-dimensional airfoil (Chatlynne et al.[12]), show that placing the synthetic jet upstream of the obstruction (thus upstream of the separation point) is not effective, and at some radial locations it results in an increase in the separated region. These results also suggest that in order to achieve a significant effect on the aerodynamic performance of the stator vane (and consequently to modify the flow within the duct) the synthetic jet actuation must be placed downstream of the obstruction. Similar results were obtained at the higher rotation speed ($\omega = 6200$ rpm, not shown).

Wake Measurements

The modification of the flow around the stator vane is accompanied by substantial changes in the structure of the stator vane wake,

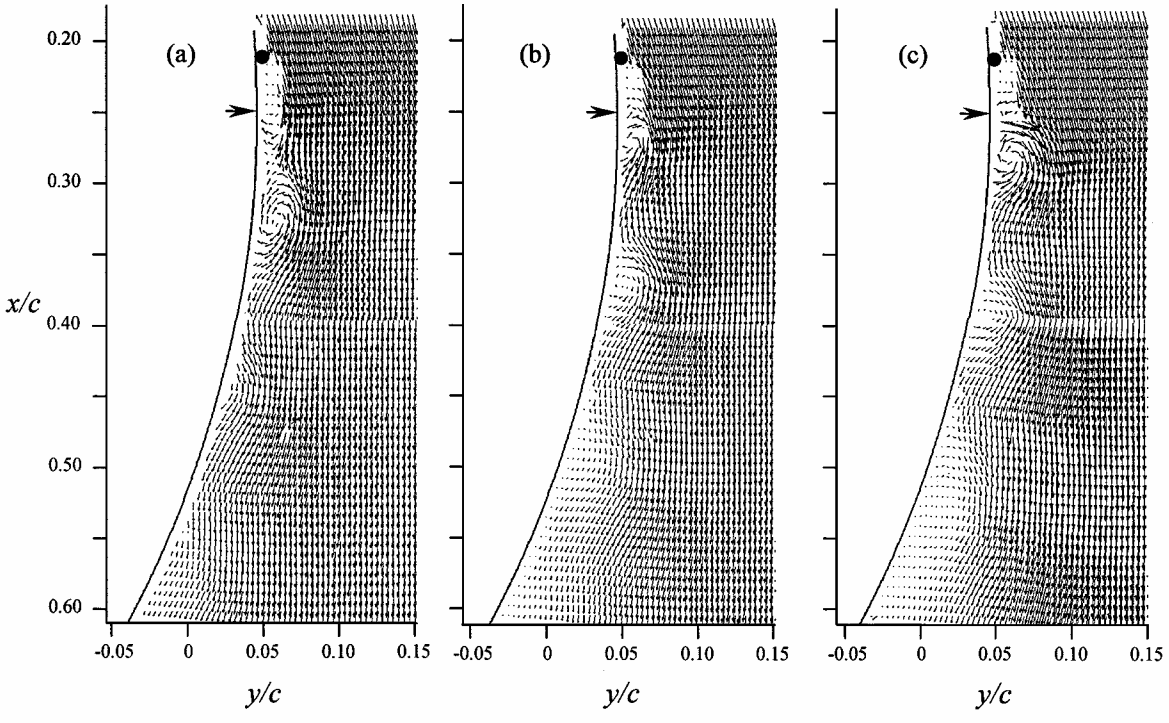

Fig. 9 Phase-averaged cross-stream maps of the velocity vectors for the actuated configurations with obstruction at $x_0/c = 0.21$, $x_j/c = 0.25$, and $\omega = 4300$ rpm: a) $\phi = 0$ deg, b) $\phi = 180$ deg, and c) $\phi = 252$ deg.

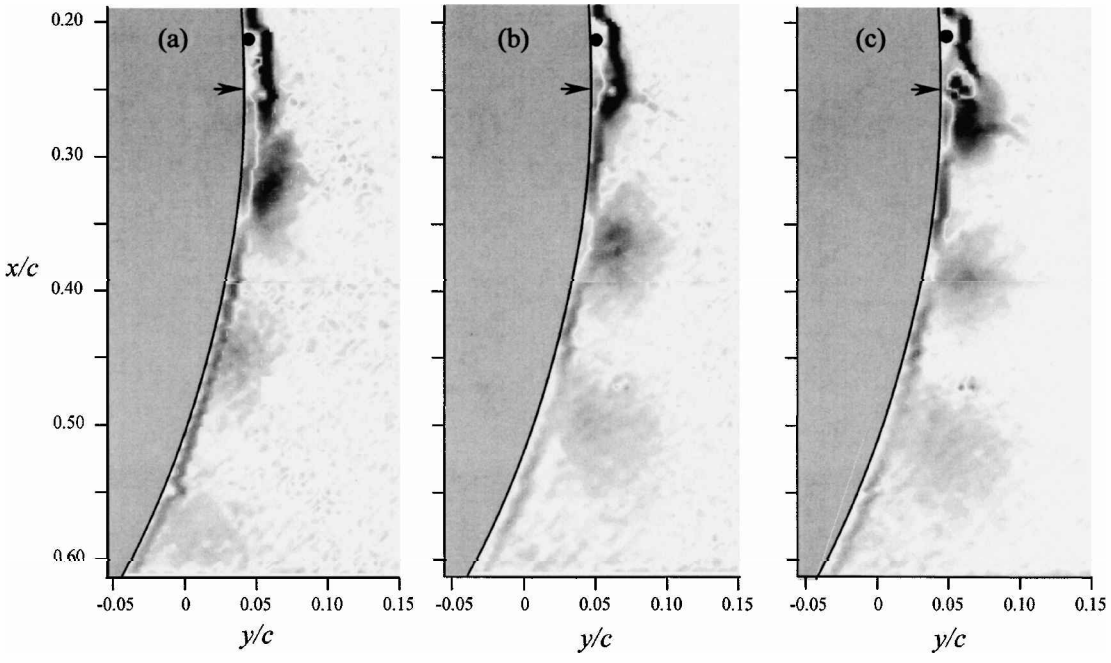

Fig. 10 Phase-averaged cross-stream maps of the spanwise vorticity for the actuated configurations with obstruction at $x_0/c = 0.21$, $x_j/c = 0.25$, and $\omega = 4300$ rpm: a) $\phi = 0$ deg, b) $\phi = 180$ deg, and c) $\phi = 252$ deg.

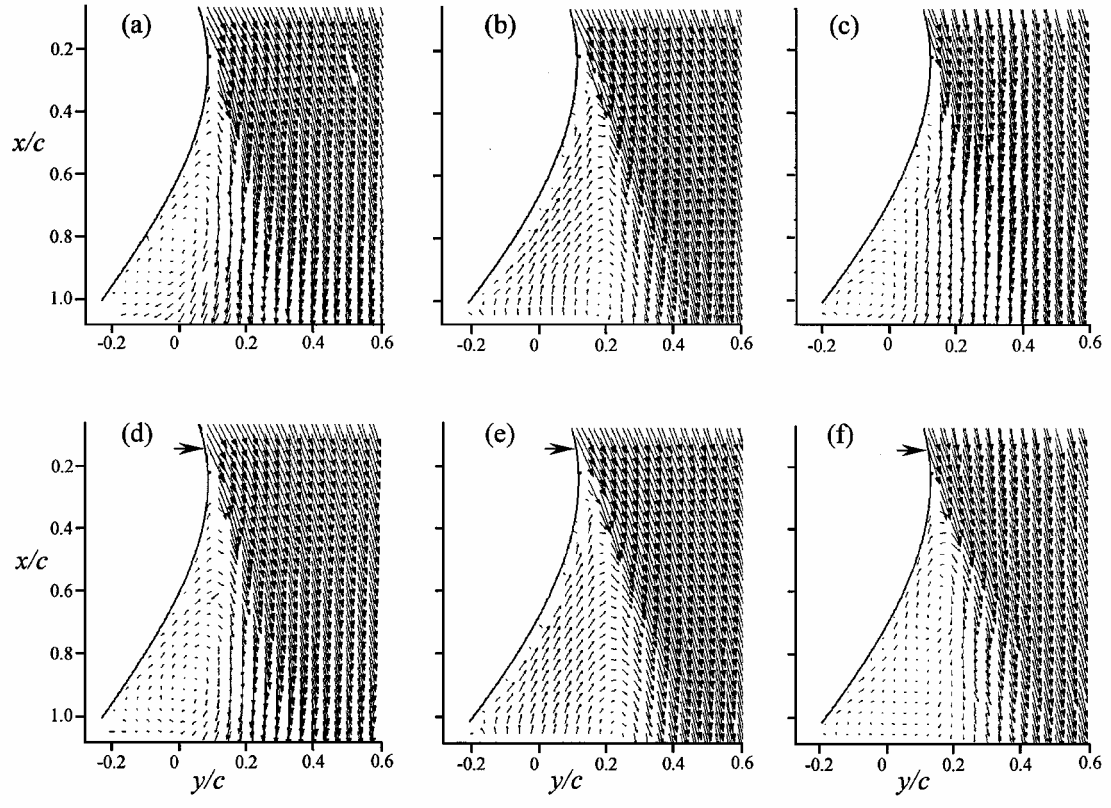

Fig. 11 Cross-stream maps of the velocity vectors with obstruction at $x_0/c = 0.21$ and $\omega = 4300$ rpm. Baseline: a) $r/R = 0.26$, b) 0.44, c) 0.70; actuated at $x_j/c = 0.14$: d) $r/R = 0.26$, e) 0.44, and f) 0.70.

which are studied using PIV in the near field ($1.5 < x/c < 2.1$ downstream from the leading edge) for $\omega = 4300$ and 6200 rpm. As in the preceding data sets, the angle of attack of the stator vane is fixed at 10 deg, the obstruction size is $0.01 \cdot c$, $x_0/c = 0.21$, and the synthetic jet is located downstream from the obstruction at $x_j/c = 0.25$. The nominally three-dimensional flowfield along the radial direction of the stator is computed from a sequence of PIV images that are captured at the same eight radial locations that were measured earlier over the suction side of the stator vane.

Figures 12a–12c show the baseline velocity vector fields in the near wake of the airfoil at $r/R = 0.26$, 0.44, and 0.70, respectively. The wake deficit is shown to be asymmetrical because of the asymmetry of the stator profile. The wake deficit and its cross stream extend increases with increasing radial distance except at $r/R = 0.70$, which shows a slight decrease in the size of the wake deficit. This could be attributed to its closeness to the duct wall or to the vortices that are shed from the propeller tip and induce downwash that decreases the separation. At $r/R = 0.26$ (Fig. 12a) the velocity vectors

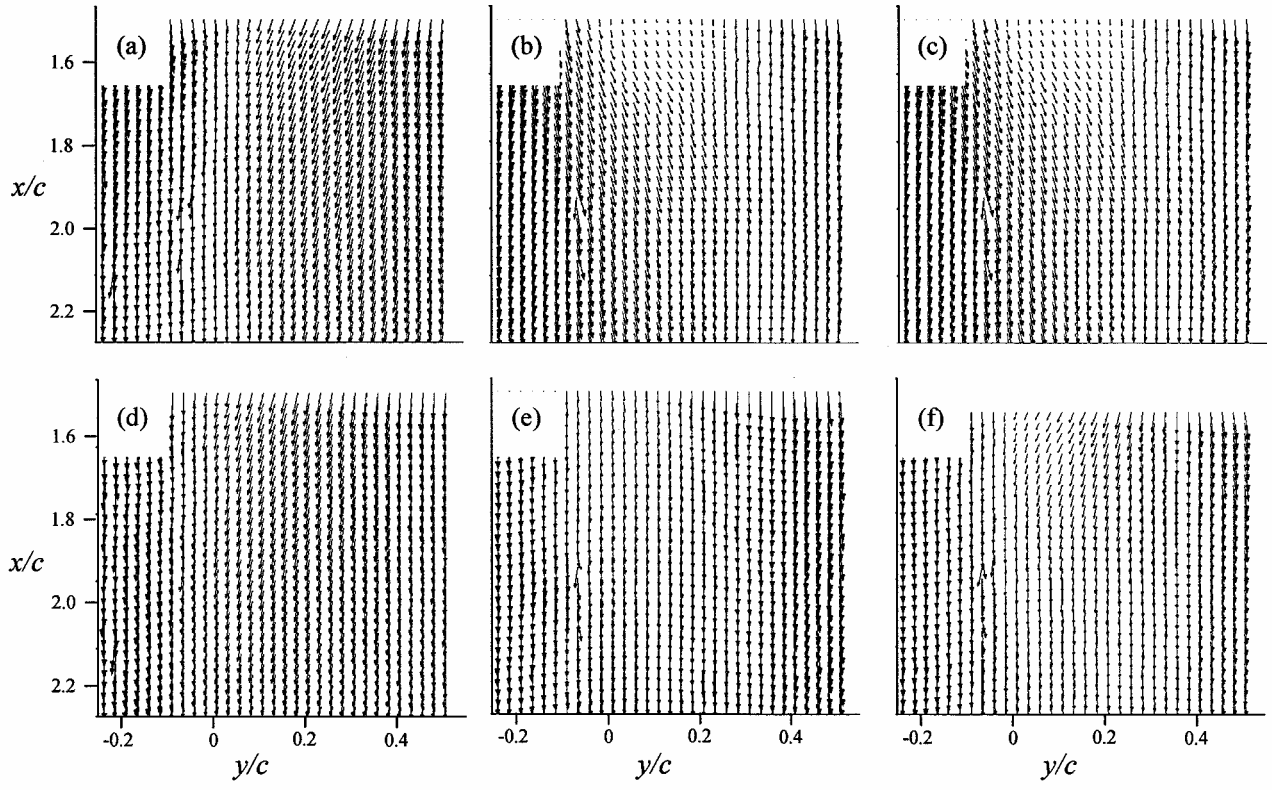

Fig. 12 Time-averaged cross-stream maps of velocity vectors in the near wake with obstruction at $x_0/c = 0.21$ and $\omega = 4300$ rpm. Baseline: a) $r/R = 0.26$, b) 0.44, c) 0.70; actuated at $x_j/c = 0.25$: d) $r/R = 0.26$, e) 0.44, and f) 0.70.

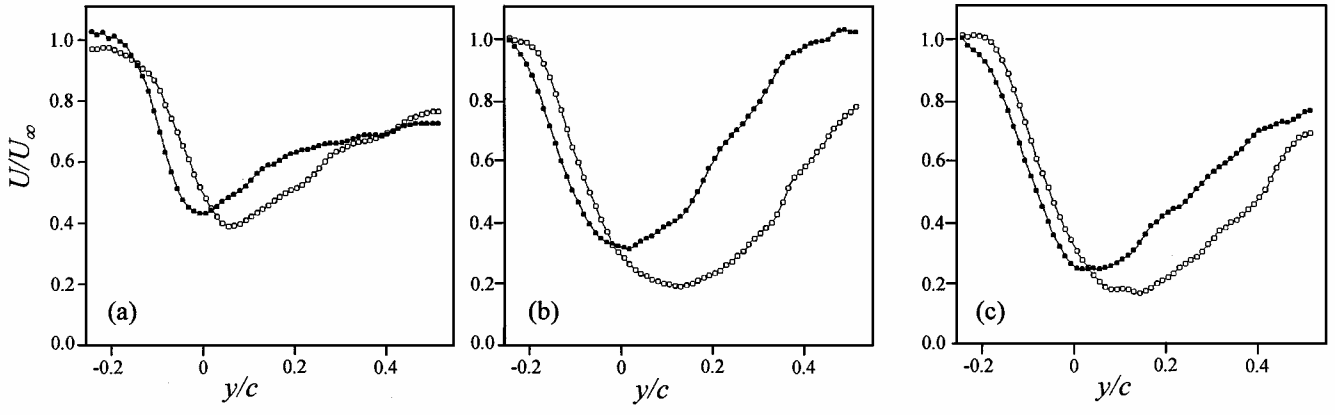

Fig. 13 Cross-stream distribution of the normalized streamwise velocity in the near wake at $x/c = 1.6$ for the baseline (○) and actuated (●) configurations with obstruction at $x_0/c = 0.21$, $x_j/c = 0.25$, and $\omega = 4300$ rpm: a) $r/R = 0.26$, b) 0.44, and c) 0.70.

on the right side of the wake deficit are tilted inward (toward the stator surface), which is an indication of an attached flow. At the other locations (Figs. 12b and 12c) the velocity vectors are tilted away from the stator surfacing, suggesting that the flow is at least partially separated.

When the control is applied (Figs. 12d–12f), the cross-stream extent of the wake and its deficit become smaller, and the wake is shifted to the negative cross-stream direction (negative y/c). For example, at $r/R = 0.44$ (Fig. 12e) the actuated wake deficit at $x/c = 1.5$ decreases from $U/U_\infty = 0.19$ to 0.31, and the cross-stream extent of the wake decreases from $0.56 \cdot c$ to $0.41 \cdot c$. This suggests that the drag coefficient is reduced while the lift coefficient is increased. Furthermore, the velocity vectors are more aligned with the freestream flow. Interestingly, at $r/R = 0.70$ actuation results in a smaller wake deficit, and the velocity vectors are tilted towards the stator surface. This somewhat contradicts the velocity data over the stator at this location, where actuation does not have an effect of the flowfield above the stator.

From the PIV data the cross-stream distributions of the velocity components at a given downstream location can be extracted. The cross-stream distributions of the streamwise velocity component at $x/c = 1.6$ (downstream from the leading edge) and at $\omega = 4300$ rpm are shown in Figs. 13a–13c for $r/R = 0.26$, 0.44, and 0.70, respectively. At all radial locations the wake of the baseline wake (open symbols) is nonsymmetric, where the right-hand side of the wake (the suction side) is much larger compared to the left side. This is caused by the nonsymmetric shape of the Clark-Y airfoil at this angle of attack. Actuation (solid symbols) results in a significant alteration of the stator wake. At $r/R = 0.26$ (Fig. 13a), where the baseline flow is shown to be attached to the stator surface (Fig. 6a), actuation has only a slight effect on the distribution. The actuated flow (Fig. 13a) shows a slight decrease in the wake deficit (decrease of drag), and the wake is shifted slightly to the left (increase in lift). At the other locations where the flow is shown to be separated (see Figs. 6b and 6c), actuation yields a significantly reduced wake deficit, and the wake is shifted to the left. At $r/R = 0.44$ (Fig. 13b)

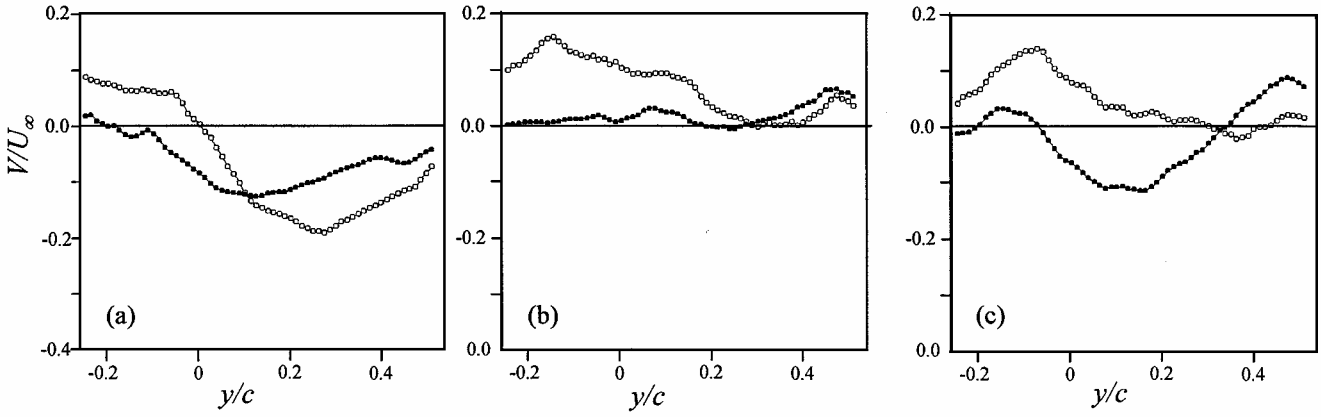

Fig. 14 Cross-stream distribution of the normalized cross-stream velocity in the near wake at $x/c = 1.6$ for the baseline (○) and actuated (●) configurations with obstruction at $x_0/c = 0.21$, $x_j/c = 0.25$, and $\omega = 4300$ rpm: a) $r/R = 0.26$, b) 0.44, and c) 0.70.

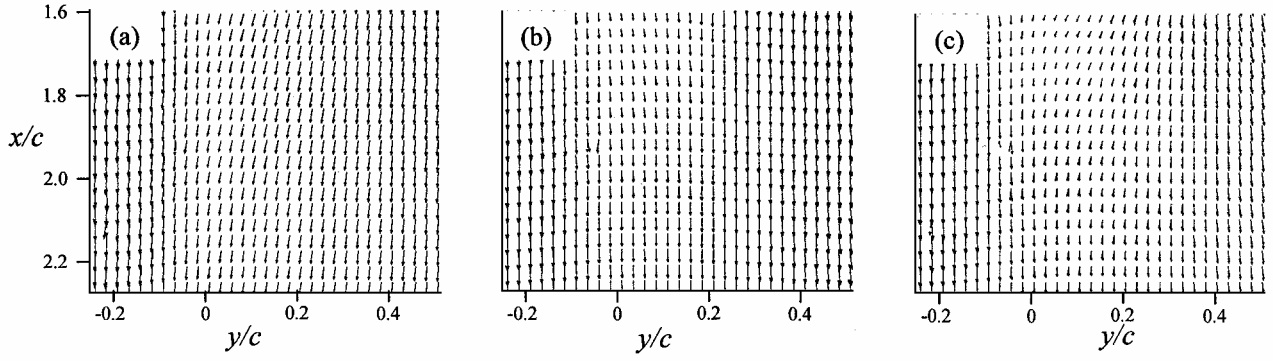

Fig. 15 Cross-stream maps of the velocity vectors in the actuated wake with obstruction at $x_0/c = 0.21$ and $\omega = 4300$ rpm: a) $r/R = 0.26$, b) 0.44, and c) 0.70: ——, time-averaged; and - - -, phase-averaged.

the peak velocity deficit is reduced from $U/U_\infty = 0.19$ to 0.31, and it is shifted from $y/c = 0.12$ to 0.01. These data complement an earlier finding (Figs. 6d–6f) that actuation at these radial locations results in flow reattachment. At $r/R = 0.70$ (Fig. 13c) actuation yields a similar but smaller effect than at $r/R = 0.44$.

Cross-stream distributions of the normalized cross-stream velocity component in the wake at $x/c = 1.6$ for the baseline and actuated flows are shown in Figs. 14a–14c ($r/R = 0.26$, 0.44, and 0.70, respectively). At $r/R = 0.26$ (Fig. 14a), where the flow is on the verge of separation (Fig. 6a), there are two regions in the cross-stream velocity distribution: for $y/c < 0$ the cross-stream velocity is positive (upwash), and for $y/c > 0$ the cross-stream velocity is negative (downwash). When actuation is applied, the cross-stream velocity becomes negative throughout most of the wake (except for $y/c < -0.18$, where the velocity is approximately zero). The downwash is larger (more negative) than in the baseline flow for $y/c < 0.11$ and smaller thereafter. The cross-stream extent of the region where the downwash of the actuated flow is smaller than that of the baseline flow increases as the radial distance increases. At $r/R = 0.44$ (Fig. 14b) this region extends to $y/c < 0.3$, whereas at $r/R = 0.70$ (Fig. 14c) the region where the cross-stream velocity is smaller for the actuated flow decreases to $y/c < 0.35$.

As just shown (Figs. 9a–9c and 10a–10c), actuation results in the formation and advection of coherent vortical structures. However, these coherent structures appear to lose their phase coherence (relative to the actuation waveform) around $x/c = 0.42$, which suggests that the wake behind the stator vane is quasi-steady. To validate this assumption, the wake in the near field is measured phase-locked to the actuation signal and compared to the time-averaged wake. Figures 15a–15c present the superimposed time-averaged and phase-averaged velocity vector fields in the near wake of the stator vane for $r/R = 0.26$, 0.44, and 0.70, respectively. Clearly, the time-averaged and phase-averaged vector fields are indistinguishable suggesting that the wake behind the stator vane is indeed quasi-steady.

Conclusions

In the work reported here, the control of the flow around a fixed stator vane of a ducted-fan UAV using synthetic jet actuators is studied experimentally. The synthetic jet actuator is actuated at 1040 Hz and $c_{\mu_{av}}$ of 1.84×10^{-3} ($\omega = 4300$ rpm) and 8.8×10^{-4} ($\omega = 6200$ rpm). The flowfields around the stator vane are measured using the particle image velocimetry (PIV) technique. The "natural" (no obstruction) flow over the stator vane at $\alpha = 10$ deg is attached to the surface; therefore, actuation resulted in a minute effect. Consequently, the flow is deliberately separated by placing a miniature ($0.01 \cdot c$) passive obstruction on the upper surface of the vane. (This technique results in a smaller loss than increasing the angle of attack to force the flow to separate naturally.) Then, a synthetic jet actuator (placed downstream of the obstruction) is used to reattach the flow.

The global view of the natural baseline (that is, no obstruction) flowfield around the stator vane show that without control the flow is completely attached at radial locations nearest to the center of the UAV and is slightly separated near the trailing edge at increasing radial locations. Actuation at either $x_j/c = 0.14$ or 0.25 results in no changes at radial locations where the baseline flow is attached and a slight delay in separation (that is, separation point moved downstream) at other locations. Qualitatively, similar results are obtained at both $\omega = 4300$ and 6200 rpm.

To force separation, a miniature passive obstruction is placed at either $x_0/c = 0.21$. The effects of the location of the obstruction as well as the location of the synthetic jet were also addressed. The best results are obtained when the obstruction is placed at $x_0/c = 0.21$ with the jet located downstream of the obstruction at $x_j/c = 0.25$. For this configuration actuation yields either complete or partial

reattachment along the span of the stator vane. Detailed views of the flowfield around the obstruction and synthetic jet showed that when the jet is actuated a recirculating bubble is formed, altering the streamlines around the stator vane, which results in flow reattachment. Phase-averaged data showed the formation of CW and CCW vortices with jet actuation, which are convected downstream (and weaken as they are convected) along the surface of the stator vane and vanish before reaching the trailing edge. Placing the synthetic jet upstream of the obstruction results in either no effect on the baseline flow or an increase in the separated region, depending on the radial location.

PIV data taken in the near field wake of the stator vane show that actuation results in a significant modification of the wake structure. The streamwise and cross-streamwise velocity components in the wake show that the wake deficit is reduced with jet actuation (reduction in drag), which confirms the measurements of the flowfield above the stator vane. Furthermore, jet actuation yields a shift of the wake deficit toward the pressure side of the stator and an increase in the downwash (increase in lift).

Superposition of the time- and phase-averaged velocity vectors in the wake confirm that the vortices formed during jet actuation diminish before they reach the trailing edge of the stator vane; thus, the actuated wake is quasi-steady.

Acknowledgments

The authors would like to acknowledge a lot of useful discussions and constructive suggestions of A. Glezer and D. E. Parekh, and the help of Shayne Kondor in designing most of the experimental apparatus.

References

[1]Cycon, J. P., "Sikorsky Aircraft UAV Program," *Vertiflite*, Vol. 38, No. 3, 1992, pp. 26–30.

[2]Walsh, D., and Cycon, J. P., "The Sikorsky Cypher® UAV: A Multi-Purpose Platform with Demonstrated Mission Flexibility," 54th American Helicopter Society, May 1998, pp. 1410–1418.

[3]Lipera, L., "Micro Craft Ducted Air Vehicle," Micro Craft Inc., San Diego, Internal Report, CA, 2001.

[4]Adams, N., Biagioni, M., and Lipera, L., "A VTOL Micro Air Vehicle Design Concept and Projected Mission Utility," Micro Craft Inc., San Diego, Internal Report, CA, 2001.

[5]Brynestad, M. A., "Investigation of the Flight Control Requirements of a Half-Scale Ducted Fan Unmanned Aerial Vehicle," M.S. Thesis, Aeronautical and Astronautical Dept., Naval Postgraduate School, Monterey, CA, March 1992.

[6]Moran, P. J., "Control Vane Guidance for a Ducted-Fan Unmanned Air Vehicle," M.S. Thesis, Aeronautical and Astronautical Dept., Naval Postgraduate School, Monterey, CA, June 1993.

[7]Kondor, S., and Heiges, M., "Active Flow Control for Control of Ducted Rotor System," AIAA Paper 2001-0117, Jan. 2001.

[8]Smith, B. L., and Glezer, A., "The Formation and Evolution of Synthetic Jets," *Physics of Fluids*, Vol. 10, No. 9, 1998, pp. 2281–2297.

[9]Smith, D. R., Amitay, M., Parekh, D., and Glezer, A., "Modification of Lifting Body Aerodynamics Using Synthetic Jet Actuators," AIAA Paper 98-0209, Jan. 1998.

[10]Amitay, M., Smith, B. L., and Glezer, A., "Aerodynamic Flow Control Using Synthetic Jet Technology," AIAA Paper 98-0208, Jan. 1998.

[11]Amitay, M., Smith, D. R., Kibens, V., Parekh, D. E., and Glezer, A., "Aerodynamic Flow Control over an Unconventional Airfoil Using Synthetic Jet Actuators," *AIAA Journal*, Vol. 39, No. 3, 2001, pp. 361–370.

[12]Chatlynne, E., Rumigny, N., Amitay, M., and Glezer, A., "Virtual Aero-Shaping of a Clark-Y Airfoil Using Synthetic Jet Actuators," AIAA Paper 2001-0732, Jan. 2001.

[13]Amitay, M., Horvath, M., Michaux, M., and Glezer, A., "Virtual Aerodynamic Shape Modification at Low Angles of Attack Using Synthetic Jet Actuators," AIAA Paper 2001-2975, June 2001.

[14]Amitay, M., and Glezer, A., "Effect of Forcing Frequency on the Aerodynamic Flow Control of a Thick Airfoil Using Synthetic Jet Actuators," *AIAA Journal*, Vol. 40, No. 2, 2002, pp. 209–216.

[15]Honohan, A. M., Amitay, M., and Glezer, A., "Aerodynamic Control Using Synthetic Jets," AIAA Paper 2000-2401, June 2000.